The Astrophysical Journal, 934:99 (15pp), 2022 August 1 https://doi.org/10.3847/1538-4357/ac7874

Neutrino Emissivities as a Probe of the Internal Magnetic Fields of White Dwarfs

Marco Drewes[1], Jamie McDonald[1], Loïc Sablon[1], and Edoardo Vitagliano[2]
[1] Centre for Cosmology, Particle Physics and Phenomenology (CP3), Université catholique de Louvain, Chemin du Cyclotron 2 B-1348 Louvain-la-Neuve Belgium
[2] Department of Physics and Astronomy, University of California Los Angeles, 475 Portola Plaza, Los Angeles, CA 90095-1547, USA; edoardo@physics.ucla.edu
Received 2021 October 14; revised 2022 June 7; accepted 2022 June 12; published 2022 July 28

Abstract

The evolution of white dwarfs (WDs) depends crucially on thermal processes. The plasma in their core can produce neutrinos that escape from the star, thus contributing to the energy loss. While in the absence of a magnetic field the main cooling mechanism is plasmon decay at high temperature and photon surface emission at low temperature, a large magnetic field in the core hiding beneath the surface even of ordinary WDs, and undetectable to spectropolarimetric measurements, could potentially leave an imprint in the cooling. In this paper, we revisit the contribution to WD cooling stemming from neutrino pair synchrotron radiation and the effects of the magnetic field on plasmon decay. Our key finding is that even if observations limit the magnetic field strength at the stellar surface, magnetic fields in the interior of WDs—with or without a surface magnetic field—can be strong enough to modify the cooling rate, with neutrino pair synchrotron emission being the most important contribution. This effect may not only be relevant for the quantification and interpretation of cooling anomalies, but suggests that the internal magnetic fields of WDs should be smaller than $\sim 6 \times 10^{11}$ G, slightly improving bounds coming from a stability requirement. While our simplified treatment of the WD structure implies that further studies are needed to reduce the systematic uncertainties, the estimates based on comparing the emissivities illustrate the potential of neutrino emission as a diagnostic tool to study the interior of WDs.

Unified Astronomy Thesaurus concepts: White dwarf stars (1799); Stellar magnetic fields (1610); Stellar properties (1624)

1. Introduction and Review

Approaching the endpoint of their evolution, stars with masses of up to several solar masses become white dwarfs (WDs). At this stage, the typical mass of the remnant of a once shining star is comparable to the solar mass, $M \sim 0.6\,M_{\odot}$, compressed in a radius similar to that of Earth. As in WDs there is no burning nuclear fuel holding up against gravitation, and the star would undergo collapse if it were not for the electron degeneracy pressure, as identified in a seminal paper by Fowler (1926). Therefore, while the mass of the star is mostly due to the nuclei, the main contribution to the pressure comes from the electrons. In most WDs, the density is such that electrons are still nonrelativistic, and only for rarer large masses can one not neglect the relativistic corrections to the equation of state, until approaching the Chandrasekhar limit (Chandrasekhar 1931).

Owing to their high density, WDs can host very strong magnetic fields. The magnetic field at the surface of a WD can be inferred from spectropolarimetric measurements. It turns out that 20% of WDs are known to be magnetic, with fields ranging on the surface from 10^4–10^8 G (see, e.g., Liebert et al. 2003; Landstreet et al. 2015; Landstreet & Bagnulo 2019; Ferrario et al. 2020). However, the magnetic field in the core of WDs is very poorly constrained and can be much stronger than at the surface. For example, *even ordinary* WDs could potentially have internal magnetic fields as large as 10^{12} G (Shapiro & Teukolsky 1983) or even larger for heavy mass WDs (Bera & Bhattacharya 2014; Franzon & Schramm 2015). Possibly, one of the only few ways to constrain the internal magnetic field of WDs is the requirement of the star to be stable through a simple argument first introduced in Chandrasekhar & Fermi (1953).

Besides affecting the structure of the WD, such strong magnetic fields could modify the cooling of the star, which depends on the local properties. Many of the processes that contribute to the cooling involve the emission of neutrinos, which can escape from regions deep inside the WD. This makes the rate of cooling an observable that is sensitive to the properties of the interior of the WD, which is hidden from direct observation. In nonmagnetic WDs, the cooling proceeds roughly through two different stages.[3] When the WD is hot, the main cooling mechanism is through the decay of plasmons, the excitations of the electromagnetic fields in the medium, to neutrinos (Winget et al. 2004; Kantor & Gusakov 2007).[4] The latter is allowed by the dispersion relations of the photons in a medium, which for transverse excitations in the nonrelativistic approximation gives photons a thermal mass (Adams et al. 1963; Zaidi 1965; Braaten & Segel 1993; Haft et al. 1994). As the WD gets colder, neutrino emission is suppressed and it cools down through the surface emission of photons. A large magnetic field can potentially catalyze the cooling by modifying the ordinary processes of a nonmagnetized core (Canuto et al. 1970a, 1970b; Galtsov & Nikitina 1972; DeRaad et al. 1976; Skobelev 1976; Kennett & Melrose 1998), and introducing additional processes as the neutrino pair synchrotron radiation (Landstreet 1967; Iakovlev & Tschaepe 1981; Kaminker et al. 1992), i.e., the emission of neutrinos by electrons scattering on external magnetic fields. We will show that the largest impact of the magnetic field on cooling is due to synchrotron radiation.

[3] In the following, we use *nonmagnetic WDs* to indicate WDs with no magnetic field both on the surface and in the core.
[4] We call *plasmon* any excitation of the electromagnetic field, making no distinction between the polarization nature of them.

In this paper, we examine the impact of magnetic fields in the interior of WDs on their cooling rates, which is limited both at the population level via the white dwarf luminosity function (WDLF) and at the level of individual stars via pulsation measurements. Our main goal is to explore the possibility of imposing upper bounds on the magnitude of the magnetic fields. In addition, we comment on the possibility that magnetic fields can account for several anomalies in the observed cooling of WDs. We summarize the effects of magnetic fields on WD cooling in Figure 5.

Constraining the magnetic field in degenerate stars complements several recent observations. Astrometric measurements suggest that most red giants (RGs), i.e., stars with compact energy sources at the center and a large convective envelope (e.g., with a large convective envelope surrounding a thin hydrogen-burning shell and a degenerate helium core), could host very large magnetic fields (Fuller et al. 2015; Cantiello et al. 2016; Stello et al. 2016), with these magnetic fields buried under the He raining down from the H-burning shell. Any magnetic field would then stay hidden below the envelope due to its long diffusion ohmic timescale. Similarly, WDs could also hide large magnetic fields beneath their surface (Cantiello et al. 2016).

From a fundamental physics point of view, there has been an ever-growing interest in the use of stars as laboratories of particle physics (Raffelt 1996), e.g., in the context of feebly interacting particles (Agrawal et al. 2021). In the realm of weakly interacting slim particles (WISPs; Arias et al. 2012), astrophysical environments like RGs and WDs have helped define constraints in the parameter space of these new particles (see Raffelt 1996; Di Luzio et al. 2020 for reviews). WISPs may also account for the total fraction of observed dark matter when produced, e.g., through the misalignment mechanism (Abbott & Sikivie 1983; Dine & Fischler 1983; Preskill et al. 1983) and potentially solve other problems plaguing the Standard Model (SM) of particle physics (e.g., the QCD axion, defined by its coupling to gluons, can explain the smallness of CP violation in the strong sector, solving the so-called strong CP problem Peccei & Quinn 1977; Dine et al. 1981).[5] Crucially, several astrophysical systems show a mild preference for an additional cooling channel (Giannotti et al. 2016, 2017). The bulk of these observations constitutes the so-called *star cooling excess*, and it has been advocated to be a hint of existing WISPs (see, e.g., Isern et al. 1992 for an early speculation). However, the stellar cooling excess is a discrepancy between the predicted and observed energy losses. As claims of physics beyond the SM should require scrutiny of SM solutions, one has to check for any possible enhancement of the predicted energy loss due to overlooked effects, e.g., a large magnetic field hiding beneath the surface of degenerate stars.

The present study is also motivated by the rapidly improving situation on the observational side. As WDs have extinguished all the nuclear fuel in their core, their temperature evolution is determined solely by cooling. WDs can be studied through different observables: both single stars and the WDLF (see, e.g., Liebert et al. 1988) can be used to study their cooling. The advent of cosmological surveys like the Sloan Digital Sky Survey (SDSS; see, e.g., Harris et al. 2006; Munn et al. 2017) and the Super COSMOS Sky Survey (Rowell & Hambly 2011) greatly improved the precision of the luminosity function as the sample size increased to several thousands of stars.

The paper is structured as follows. In Section 2, we briefly summarize the cooling of WDs obtained assuming a non-magnetized plasma in the core. In Section 3.1, we revisit the idea of a large magnetic field in the core. Then, we will show how the magnetic field implies both the modification of plasmon decay, described in Section 3.2, and the possibility for electrons to radiate neutrinos through synchrotron radiation, discussed in Section 3.3. This will bring us to our conclusions.

2. Cooling in Absence of Magnetic Fields

Before investigating the effect of magnetic fields on WD cooling, and in order to put our results into context, we briefly review the most important cooling mechanisms that do not rely on magnetic fields.

2.1. Cooling through Plasmon Processes

The hottest and brightest WDs correspond to the younger ones. During this stage, the dwarf cools mostly through neutrino emission. The dominant emission is from plasmon decay (Kantor & Gusakov 2007), with other processes like bremsstrahlung coming far second (Winget et al. 2004). Plasmon decay in a nonmagnetized medium has been extensively studied in the literature (Adams et al. 1963; Zaidi 1965), with the most comprehensive treatment given by the seminal paper of Braaten & Segel (1993), which we use as the basis of our calculations. Explicitly, for the energy regimes relevant to stellar cooling, plasmon processes proceed via Fermi interactions,

$$\mathcal{L}_{\rm int} = \frac{G_{\rm F}}{\sqrt{2}}\, \bar{e}\gamma^{\mu}(C_{\rm V} - C_{\rm A}\gamma_5)e\; \bar{\nu}_a\gamma_{\mu}(1-\gamma_5)\nu_a, \tag{1}$$

where $G_{\rm F} = 1.166 \times 10^{-5}\,{\rm GeV}^{-2}$ is the Fermi constant and e and ν_a are spinors representing electrons and neutrinos of flavor $a = e,\ \mu,\ \tau$, respectively. The effective vector (V) and axial-vector (A) coupling constants include both neutral current and charged current. Altogether one finds

$$C_{\rm V} = \tfrac{1}{2}(4\sin\Theta_{\rm W} + 1) \quad \text{and} \quad C_{\rm A} = +\tfrac{1}{2} \quad \text{for } \nu_e, \tag{2a}$$

$$C_{\rm V} = \tfrac{1}{2}(4\sin\Theta_{\rm W} - 1) \quad \text{and} \quad C_{\rm A} = -\tfrac{1}{2} \quad \text{for } \nu_\mu,\ \nu_\tau \tag{2b}$$

in terms of the weak mixing angle $\Theta_{\rm W}$. One can obtain the squared matrix element for the transition $\gamma \to \bar{\nu}\nu$ and compute the decay rate

$$\Gamma_{\gamma\to\nu\bar{\nu}}(\omega) = \int \frac{d^3\boldsymbol{k}_{\nu}}{(2\pi)^3 2\omega_{\nu}} \frac{d^3\boldsymbol{k}_{\bar{\nu}}}{(2\pi)^3 2\omega_{\bar{\nu}}} \frac{|\mathcal{M}_{\gamma\to\nu\bar{\nu}}|^2}{2\omega} \times (2\pi)^4\,\delta^4(k - k_{\nu} - k_{\bar{\nu}}), \tag{3}$$

where $k_{\nu,\bar{\nu}} = (\omega_{\nu,\bar{\nu}}, \boldsymbol{k}_{\nu,\bar{\nu}})$ and $(\omega,\ k)$ are the wavevectors of outgoing neutrinos and incoming photons, and $\mathcal{M}$ the relevant scattering amplitude. The energy loss (per volume per unit time) for each polarization can be computed as

$$Q_{\gamma\to\nu\bar{\nu}} = \int \frac{d^3\boldsymbol{k}}{(2\pi)^3}\omega\Gamma_{\gamma\to\nu\bar{\nu}}(\omega) f_B(\omega), \tag{4}$$

where $f_B(\omega) = 1/(e^{\omega/T} - 1)$ is the Bose–Einstein distribution evaluated at the plasmon energy $\omega = \omega_t,\ \omega_l$ given in Appendix A. Integrating the energy loss over the star volume, one obtains the luminosity. We can identify three contributions

[5] Note that it has recently been put into question in Ai et al. (2021) whether there actually is a strong CP problem in the SM.

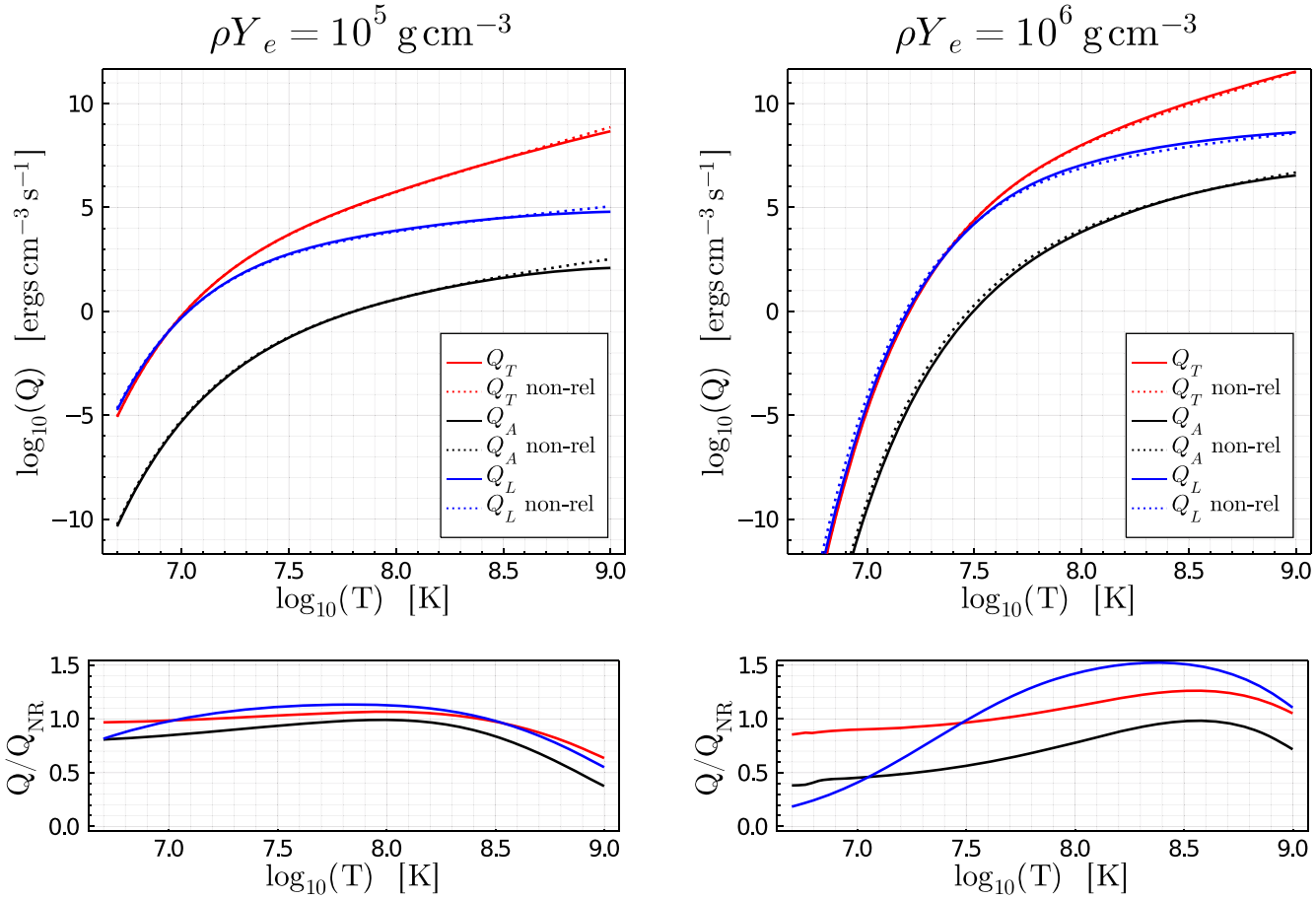

Figure 1. Plasmon decay emissivities. The emissivities in an unmagnetized medium for plasmon decay for the transverse (Q_T), longitudinal (Q_L), and axial (Q_A) processes. We show both the full emissivities in Equations (5a)–(5c) (solid lines) and the nonrelativistic limits (dotted lines) for Q_T and Q_A given by the integrals in Equations (A18) and (A20), respectively. The bottom panel shows the ratio of the full to nonrelativistic emissivities.

to the plasmon emissivity $Q_{\gamma\to\nu\bar{\nu}}$, which depend on the polarization of the photon and whether the process is due to the axial vector or the vector coupling. These are, calling the fine structure constant $\alpha = e^2/4\pi$,

$$Q_T = 2\left(\sum_{\nu_\alpha} C_V^2\right)\frac{G_F^2}{96\pi^4\alpha}\int_0^{+\infty} \times dk\ k^2 Z_t(k)(\omega_t^2 - k^2)^3 f_B(\omega_t), \tag{5a}$$

$$Q_A = 2\left(\sum_{\nu_\alpha} C_A^2\right)\frac{G_F^2}{96\pi^4\alpha}\int_0^{+\infty} \times dk\ k^2 \Pi_A(\omega_t, k)^2 Z_t(k)(\omega_t^2 - k^2) f_B(\omega_t), \tag{5b}$$

$$Q_L = \left(\sum_{\nu_\alpha} C_V^2\right)\frac{G_F^2}{96\pi^4\alpha}\int_0^{k_{\max}} \times dk\ k^2 Z_l(k)\omega_l^2(\omega_l^2 - k^2)^2 f_B(\omega_l), \tag{5c}$$

which we refer to respectively as transverse, axial, and longitudinal. Full expressions for Z_ℓ, ω_ℓ, ω_t, and Π_A can be found in Appendix A. We display the plasmon emissivities[6], Equations (5a)–(5c) in Figure 1. Note in particular the subdominance of the axial contribution. In the remainder of this paper, we make frequent use of nonrelativistic approximations characterized by $p \ll m_e$ and $T \ll m_e$, where p is a typical electron momentum and m_e is the electron mass. For consistency, we examine in Appendix A.2 to what extent the relativistic results for plasmon cooling. Equations (5a)–(5c) are well approximated by their nonrelativistic limits for the parametric regimes relevant for WDs, thereby providing a cross check that relativistic corrections can be reasonably neglected in the remainder of the paper.

[6] Notice that Figure 2 of Braaten & Segel (1993) seems to report an incorrect axial-vector flux, as observed in Kohyama et al. (1994).

2.2. Cooling through Photon Surface Emission

At colder temperatures, WDs cool predominantly through photon surface emission. This can be estimated by Mestel's cooling law (Kaplan 1950; Mestel 1952; Shapiro & Teukolsky 1983). As the interior of the star is degenerate, electrons have a long mean free path. Therefore, there is a roughly homogeneous temperature all over the core (see, for example, Figure 1 of Bischoff-Kim et al. 2008 and Figure 4 of Córsico et al. 2014). On the other hand, the external layers are nondegenerate and are in radiative equilibrium. Thus, one can show that for typical values of a WD, the emission from the nondegenerate external layer is approximately determined by the temperature T in the transition region between the degenerate core and the nondegenerate external layers, approximately equal to the central temperature (Shapiro & Teukolsky 1983),

$$L_\gamma \simeq (2 \times 10^6 \text{ erg s}^{-1}) \frac{M}{M_\odot} T^{3.5}, \quad (6)$$

where M is the WD mass. As noted by Mestel, this can be understood as the WD radiating away its residual ion thermal energy.[7] This is a surface emission, and therefore depends on the global properties of the star. For comparison with other rates given per unit volume, it is useful to define the following volume-averaged emissivity, obtained by dividing the left and right terms of Equation (6) by the volume,

$$Q_\gamma = \vartheta \frac{L_\odot}{M_\odot} \rho T_7^{3.5}, \quad (7)$$

where $L_\odot = 3.83 \times 10^{33}$ erg s^{-1}, $\vartheta = 1.7 \times 10^{-3}$, and $T_7 = T/10^7$ K (Raffelt 1986).[8]

After this stage, the core crystallizes, and the WD becomes fainter and fainter. The crystallization phase has been recently observed (Tremblay et al. 2019) by the Gaia satellite (Prusti et al. 2016), which could improve the accuracy of methods used to determine the age of stellar populations.

3. Magnetic Field Effects on WD Cooling

Having reviewed the standard cooling microphysics of nonmagnetic WDs via neutrinos and photons, we now proceed to study two new contributions to WD cooling: modifications to the axial emission due to the polarization of the medium by a magnetic field and neutrino emission via synchrotron processes. The final results are summarized in Figure 5.

3.1. Revisiting Large Magnetic Fields in WD Cores

The internal magnetic field B in WDs is poorly constrained by observations and could be much stronger than the one at the surface. The existence of a B field on the surface of magnetic white dwarfs (MWDs) is observed via spectroscopic measurements (Liebert et al. 2003; Landstreet et al. 2015; Landstreet & Bagnulo 2019; Ferrario et al. 2020). The presence of a large magnetic field, up to hundreds of megagauss, on the surface of MWDs had already been observed in the 1970s by detection of broadband circular and linear polarization (Kemp et al. 1970; Angel & Landstreet 1971). Another way of detecting such huge fields is by relying on the Zeeman effect, which can cause the splitting of Balmer lines (Angel & Landstreet 1970).

In this way, MWDs have been discovered with B fields of 10^3–10^9 G, in an ever-growing number, from the circa 70 in the early 2000s (Wickramasinghe & Ferrario 2000) to 600 and counting (Ferrario et al. 2015), thanks to SDSS (Kepler et al. 2013). The data suggest that 10%–20% of WDs show a surface magnetic field (see, e.g., Sion et al. 2014; Ferrario et al. 2020). However, we cannot constrain the B field in the core of WDs by spectropolarimetric observations, thus making viable the possibility of a very large magnetic field in the core, possibly even of WDs, which do not appear magnetic at the surface. The B field in the core of a WD could be as large as 10^{13} G (Angel 1978; Shapiro & Teukolsky 1983). Interestingly, MWDs in the past were considered to be WDs that got rid of the hydrogen envelope, and it was suspected that all WDs had large B fields (Imoto & Kanai 1971; Chanmugam & Gabriel 1972). However, this hypothesis has been abandoned since magnetic stars have been observed with H-dominated atmospheres. Nevertheless, it might still be the case that even WDs showing no magnetic field on their surface might host a large magnetic field in their core.

The problem of measuring the internal magnetic field arises for stars going through different stages of their lives. For example, the Sun may host a B field as large as 10^7 G, despite having a much smaller field on the surface (Couvidat et al. 2003). In the case of the Sun, bounds can come from neutrinos (as they track the temperature, and the latter would be affected by a different energy density due to the presence of a B field), and from the oblateness of the Sun itself (Couvidat et al. 2003; Friedland & Gruzinov 2004). Helioseismology can only put bounds on the magnetic field down to the tachocline (Antia et al. 2000; Baldner et al. 2009; Barnabé et al. 2017). Concerning the core of RGs, a progenitor of WDs, the presence of strong magnetic fields (in excess of 10^5 G or more) is inferred using asteroseismology. In Fuller et al. (2015), it is shown how certain oscillations (the so-called g-dominated mixed modes) observed at the surface of RGs are damped by the presence of a strong internal magnetic field above a critical value. This critical value turns out to be 10^5 G. In a sample of 3000 RGs (Stello et al. 2016), about 20% show the presence of suppressed dipole modes. Assuming that this reveals the presence of magnetism, 20% of RGs might possess strong internal magnetic fields. Notice that these fields are likely confined to the stellar core, and do not extend to the stellar envelope/stellar surface.

Interestingly, asteroseismological observations of RGs suggest that a large fraction of lower mass WDs might have strong internal magnetic fields (Cantiello et al. 2016). The key observation is that their magnetic fields are likely buried below the surface and not detectable via Zeeman spectropolarimetry. A few caveats are nevertheless in order. Even if strong B fields are generated by convective cores during the main sequence, it is not clear if these fields are preserved all the way to the WD formation. There are many processes that could potentially destroy the B field as the star goes, e.g., through the He flash, or other later convective phases. Moreover, a problematic issue is the stability of the magnetic field itself. Both purely poloidal and toroidal fields are dynamically unstable, even though a combination of the two could be stable (Braithwaite & Nordlund 2006; Duez et al. 2010). This field can hide under the surface, or emerge at the surface, as long as it has both a poloidal and toroidal component. As the problem of magnetic field stability is well beyond the scope of this paper, we will neglect these issues.

A final comment should be about variable stars. There is the possibility that pulsating WDs might host a large B field underneath its surface, hidden even to asteroseismology. An order of magnitude estimate is enough to show that an extremely large B field would affect the amplitude of oscillations (Cox 1980). Moreover, if B fields affect oscillations, even a small variation over time of the B field would be enormously amplified by the oscillations. The possibility of using asteroseismology to detect the B field in a pulsating WD has been questioned (Heyl 2000; Loi & Papaloizou 2018). However, we stress that very large magnetic fields should be potentially bound by asteroseismology in pulsating WDs (see also Jones et al. 1989).

[7] Notice that for magnetic fields $B \lesssim 10^{12}$ G, one can assume the effect of the magnetic field on the specific heat to be negligible (see, e.g., Baiko 2009; Bhattacharya et al. 2018).

[8] Notice that the surface emission used in Giannotti et al. (2016) is slightly smaller, so we conservatively assume a larger photon emission.

With these points in mind, the question left is to develop some understanding of the internal magnetic field structure of WDs. In Appendix B, we use virial arguments to examine an upper bound (see Equation (B8)) on the maximum strength of B that can be supported within some core regions while maintaining stellar stability. The strength of these arguments lies in their simplicity—as they are built on very basic physical principles, and thus in principle are very robust. However, by construction virial arguments can only constrain the integrated magnetic field within some regions. Applying them to the star as a whole yields a rather robust upper limit on the average value of B, which could, however, easily be avoided by much stronger fields that are localized in small regions inside the WD. Applying virial arguments to the subregions of the WD relies on a detailed understanding of its structure, leading to a loss of robustness due to modeling uncertainties. In the remainder of this section, we present an alternative way to constrain the local B in subregions of the WD, based on its impact on the neutrino emissivity.

3.2. Plasmon Decay in a Magnetized Medium

Neglecting processes that depend on the ion content (such as crystallization), a nonmagnetized QED plasma is completely described by the electron number density (or alternatively the chemical potential) and the temperature. The presence of a macroscopic magnetic field, as we will review, can affect the plasma in several ways. First, it can generate QED nonlinear effects. Moreover, it can affect the electron wave functions, and modify the propagation of the electromagnetic field excitations. Some of these effects will modify the energy loss from plasmon decay, as shown in the 1970s (Canuto et al. 1970a, 1970b; Galtsov & Nikitina 1972; DeRaad et al. 1976; Skobelev 1976). We will follow a more recent treatment that corrects for several flaws in previous works (Kennett & Melrose 1998).

QED nonlinear effects are of two kinds. On the one hand, a critical field $B_c = m_e^2/e = 4.41 \times 10^{13}$ G is so large that the macroscopic field could create electron-positron pairs. We will always consider fields smaller than this value. The second class of effects is related to the vacuum birefringence effect (Tsai & Erber 1975) as a large macroscopic field affects the refractive index, and can affect plasmon decay to neutrinos.[9] The magnetic field introduces an additional energy scale, the synchrotron frequency

$$\omega_B = \frac{eB}{m_e} = m_e \frac{B}{B_c} \simeq 11.5\, B_{12}\ \mathrm{keV}. \tag{8}$$

As a rule of thumb, one can compare how the magnetic field and the plasma modify the refractive index, respectively. The equations for vacuum birefringence are given in Tsai & Erber (1975), and reduce for $B \lesssim B_c$ to $n^2_{\mathrm{vacuum}} - 1 \simeq \kappa\alpha^2 B^2/m_e^4$, where κ is a constant that depends on the polarization ($\kappa_\parallel = 14/45$ and $\kappa_\perp = 8/45$ for the electric field parallel and perpendicular to the external magnetic field, respectively; Raffelt 1996). As the refractive index in an unmagnetized plasma is $n^2_{\mathrm{plasma}} - 1 = -\omega_p^2/\omega^2$, one finds that vacuum birefringence is negligible for (Meszaros & Ventura 1979; Pavlov et al. 1980)

$$\frac{\alpha}{4\pi}\frac{\omega_B^2}{m_e^2}\frac{\omega^2}{\omega_p^2} = \frac{\alpha}{4\pi}\frac{B^2}{B_c^2}\frac{\omega^2}{\omega_p^2} \lesssim 1, \tag{9}$$

which is safely satisfied for $\omega \simeq T$, $B \lesssim B_c$ and the range of temperatures and densities considered here, see also Equation (A17).

The most important effect that B has in the range considered here is to force electrons on Landau levels with energies (notice that $\omega_B/m_e = B/B_c$)

$$E_\nu = \sqrt{p_\parallel^2 + m_e^2\left(1 + 2\nu\frac{B}{B_c}\right)}, \tag{10}$$

with $p_\parallel$ the component of the momentum parallel to the magnetic field and $\nu = l + \frac{1}{2} + \sigma$, $l \geqslant 0$ is an integer labeling the orbital angular momentum, $\sigma = \pm\frac{1}{2}$, $g_0 = 1$, and all other $g_\nu = 2$. The electron density is then computed as (see, e.g., Lai & Shapiro 1991)

$$n_e = \frac{m_e^2}{(2\pi)^2}\frac{B}{B_c}\sum_{\nu=0}^{\infty} g_\nu \int_{-\infty}^{\infty} dp_\parallel f_-^\nu(E_\nu), \tag{11}$$

where $f_\pm^\nu = \left[\exp\left(\frac{E_\nu \pm \mu}{T}\right) + 1\right]^{-1}$ for electrons ($-$) and positrons ($+$), respectively, and we neglected positrons. In Kennett & Melrose (1998) the extreme case where only the lowest level is occupied was considered. We shall in the following investigate the impact of B on the plasmon emission rate under this extreme assumption. By doing so we overestimate the effect of B for realistic values in WDs, as one can see by estimating the magnitude of B that would be needed to confine all electrons to the lowest Landau level. To show this we make the conservative assumption $T = 0$, which yields a maximal (Fermi) momentum $p_\parallel = p_{F\parallel}(\nu)$ that is defined by the condition

$$p_{F\parallel}^2(\nu) + m_e^2\left(1 + 2\nu\frac{B}{B_c}\right) = \mu^2, \tag{12}$$

with μ the electron chemical potential. The highest occupied Landau level $\nu_{\max}$ corresponds to the maximal ν for which Equation (12) has a real solution in $p_{F\parallel}$. Hence, if we require a value for $\nu_{\max}$, we can demand $p_{F\parallel}(\nu_{\max} + 1) = 0$ to identify the largest chemical potential μ for which only Landau levels up to $\nu_{\max}$ are filled, and express

$$n_e = \frac{m_e^3}{(2\pi)^2}\left(\frac{2B}{B_c}\right)^{3/2}\sum_{\nu=0}^{\nu_{\max}} g_\nu\sqrt{1 + \nu_{\max} - \nu}. \tag{13}$$

Demanding $\nu_{\max} = 0$ leads to $n_e = m_e^3/(2\pi)^2\,(2B/B_c)^{3/2}$ or $B = \frac{1}{2}B_c(4\pi^2 n_e/m_e^3)^{2/3}$, i.e., $B/B_c \simeq 0.6$ for $Y_e\rho \simeq 10^6\ \mathrm{g\,cm^{-3}}$, where Y_e is the number of electrons per baryon. Therefore, one needs incredibly large magnetic fields to keep the electrons at the lowest Landau level. We find that the value of the B field for this to happen is much larger than the one cited in Kennett & Melrose (1998), where it was assumed that the kinetic energy of the electron was due to the temperature, rather than the Fermi energy. However, for the strongest magnetic fields

[9] This is similar to the way the Cotton–Mouton effect is known to modify photon conversion to axions (Raffelt 1996).

considered here, one still expects a sizeable fraction of the electrons in the lowest Landau levels.

As the general problem in which both the thermal motion of electrons (due to temperature or Fermi energy) and the magnetic fields are accounted for is very complicated (Melrose 1986; Kennett & Melrose 1998), we will limit ourselves to an electron cold plasma distribution, assuming that most electrons are in the lowest Landau energy level. In this way, we will be able to estimate the maximal variation in the plasmon decay neutrino flux due to the presence of the magnetic field. In particular, the effect will be large on the axial-vector coupling emission: since this is associated with coherent spin oscillations (see also Appendix A), the magnetic field breaks parity and aligns the spins, so that constructive interference is possible in the magnetized plasma for $\nu = 0$.

Even with these simplifications, as the magnetic field breaks the isotropy of the medium, the problem of finding the dispersion relations of the electromagnetic field excitations becomes rapidly complicated (Swanson 2012). Therefore, we can estimate the effect the B field has on neutrino emission from plasmon decay by considering the decay of plasmons propagating parallel or orthogonal to the magnetic field. The explicit evaluation of Equation (3) is enormously simplified by using a long-wavelength approximation for both the vector and axial-vector polarization functions, and using the Stix form for the dielectric tensor (Stix 1962; Melrose 1986; Swanson 2012) one can obtain simple expressions of the refractive index for different wavevector directions and polarizations.

Taking these facts in combination, the different plasmon emission processes in a magnetized medium can be categorized according to (i) whether they proceed via the axial-vector or vector coupling (ii) the value of θ (i.e., the direction of propagation with respect to the magnetic field) and (iii) the polarization of the mode in question, which can be oriented relative to the direction of B. Expressions for general θ are quite complicated so in order to obtain some quantitative understanding of the size of effects, we examine various special cases below taken from Kennett & Melrose (1998).

Circularly polarized parallel propagation ($\theta = 0$)—For $\theta = 0$, the axial-vector and longitudinal contribution is not modified. The remaining contribution therefore proceeds via the vector coupling resulting in an effect to a modification of Q_T. This consists of two circularly polarized modes:

$$Q_{\pm}(\theta = 0) = \frac{1}{4\pi}\left(\sum_{\nu_\alpha} C_V^2\right)\frac{G_F^2}{96\pi^4\alpha}\int_{\omega_{\rm min}}^{\infty} \times d\omega\ \omega^8 n_{\pm}(1 - n_{\pm}^2)^3 f_B(\omega), \tag{14}$$

where

$$n_{\pm}^2 = 1 - \frac{(\omega_p/\omega)^2}{1 \pm \omega_B/\omega}, \tag{15}$$

and $\omega_{\rm min}$ corresponds to the refractive index $n = k/\omega$ being equal to 0, since below this cutoff the modes do not propagate.[10] This expression coincides with the one found in Canuto et al. (1970a), and is independent of the axial-vector coupling. Note that summing $Q_{\pm}$, taking the limit of zero magnetic field, and integrating over the plasmon direction, we find again Equation (A18), as expected.

[10] Notice moreover that one should check that $n \leqslant 1$, so that the excitations are time-like.

Perpendicular propagation ($\theta = \pi/2$), *parallel polarization*—A mode propagating perpendicular to B but polarized parallel to B is known as the ordinary mode (so-called because it has the same dispersion relation as though the anisotropy were not there). Both the axial-vector and vector contributions are modified by the B field for this case, giving rise to

$$Q_o\left(\theta = \frac{\pi}{2}\right) = \frac{1}{4\pi}\frac{G_F^2}{96\pi^4\alpha}\int_{\omega_{\rm min}}^{\infty} d\omega\ \omega^8 n_o(1 - n_o^2)^2 \times \left[\left(\sum_{\nu_\alpha} C_V^2\right)(1 - n_o^2) + \left(\sum_{\nu_\alpha} C_A^2\right)n_o^2\right] f_B(\omega), \tag{16}$$

where the refractive index is independent of B,

$$n_o^2 = 1 - \left(\frac{\omega_p}{\omega}\right)^2. \tag{17}$$

Perpendicular propagation ($\theta = \pi/2$), *perpendicular polarization*—This case is referred to as the extraordinary mode (the plasma dispersion relation receives magnetic field corrections), for which the vector (but not the axial-vector) contribution is modified:

$$Q_x\left(\theta = \frac{\pi}{2}\right) = \frac{1}{4\pi}\left(\sum_{\nu_\alpha} C_V^2\right)\frac{G_F^2}{96\pi^4\alpha}\int_{\omega_{\rm min}}^{\infty} d\omega\ \omega^8 n_x(1 - n_x^2) \times \left[(S - 1)^2 + D^2 - \frac{4D^2 S(S - 1)}{D^2 + S^2}\right] f_B(\omega), \tag{18}$$

where

$$n_x^2 = \frac{S^2 - D^2}{S},\quad S = 1 - \frac{(\omega_p/\omega)^2}{1 - (\omega_B/\omega)^2},\quad D = \frac{\omega_B\omega_p^2}{\omega(\omega^2 - \omega_B^2)}. \tag{19}$$

We summarize the size of these contributions in Figure 2, which compares the plasmon processes in a magnetized medium to the plasmon processes in the unmagnetized medium. Neutrinos from plasmon decay might potentially constrain the internal B field of WDs. The colder part of the WDLF shows some excessive cooling (Giannotti et al. 2016), while the hot part does not show it (Hansen et al. 2015). Notice however that the WDLF uncertainty is large in the hottest range. From Figure 2 it can be seen that the plasmon decay is mostly modified at rather large temperatures. We will show in the next section that the emission from synchrotron radiation dominates plasmon decay for values of the magnetic field whose effect on plasmon decay is large. If in the future this part of the WDLF is measured precisely, a dedicated and computationally more challenging estimate of the B field effect on plasmon decay would be demanded, featuring, e.g., a warm plasma (Kennett & Melrose 1998).

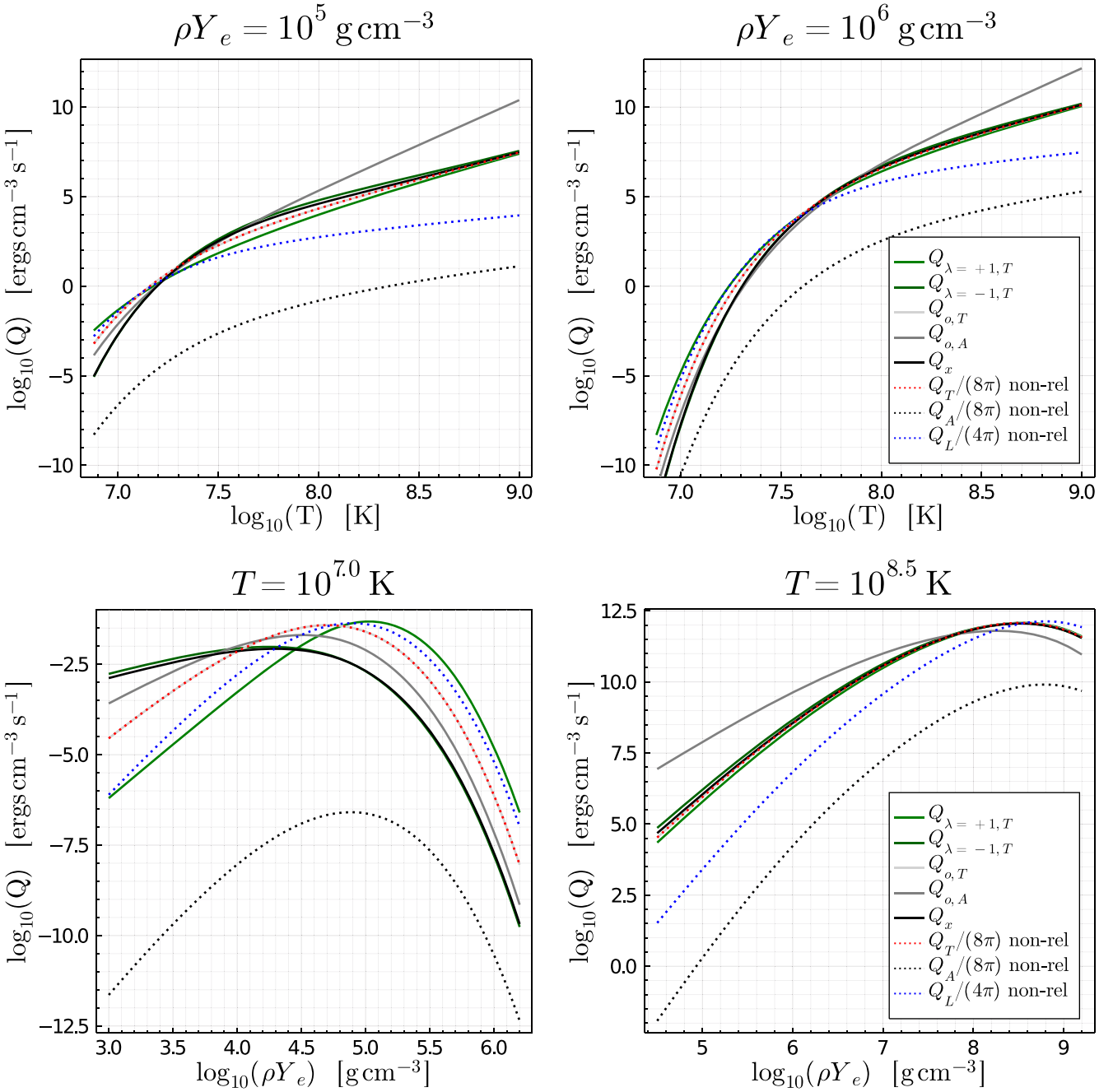

Figure 2. Magnetized plasmon emission. Effect of a strong magnetic field on the plasmon processes $\gamma \to \nu\bar{\nu}$. We show the energy loss per polarization in a magnetized plasma ($Q_\pm$, Q_O, Q_x) with solid lines, while the conventional plasmon processes in the unmagnetized medium ($Q_{T,A,L}$) are shown as dotted lines. We display the effect as a function of temperature (top row) for two densities and also as a function of varying density (bottom row) for fixed temperature and magnetic field $B = 7 \times 10^{11}$ G.

3.3. Neutrino Pair Synchrotron Radiation

Similar to neutrino production from bremsstrahlung, which is the main neutrino production channel during the surface cooling phase, synchrotron emission is possible thanks to an external field. The B field forces the electrons to rotate around the magnetic field lines. The electron momentum is not conserved, allowing for the process $e \xrightarrow{B} e\ \bar{\nu}\ \nu$. Neutrino pair synchrotron emission has been the subject of many studies, spanning several decades (see, e.g., Landstreet 1967; Iakovlev & Tschaepe 1981; Yakovlev et al. 2001). Using the notation introduced in Section 3.2, the emissivity reads as (Kaminker et al. 1992)

$$Q_{\rm syn} = \left(\sum_{\nu_\alpha} C_A^2\right) \frac{G_F^2 \omega_B^6}{30\pi^3} \frac{m\omega_B}{(2\pi)^2} \sum_{\nu=1}^{\infty} \int_{-\infty}^{+\infty} \times dp_\parallel [f_-^\nu (1 - f_-^{\nu-1}) + f_+^\nu (1 - f_+^{\nu-1})], \quad (20)$$

where as above

$$f_\pm^\nu = \left[\exp\left(\frac{E_\nu \pm \mu}{T}\right) + 1\right]^{-1},$$
$$E_\nu = \sqrt{p_\parallel^2 + m_e^2 + 2\nu\omega_B m_e}. \quad (21)$$

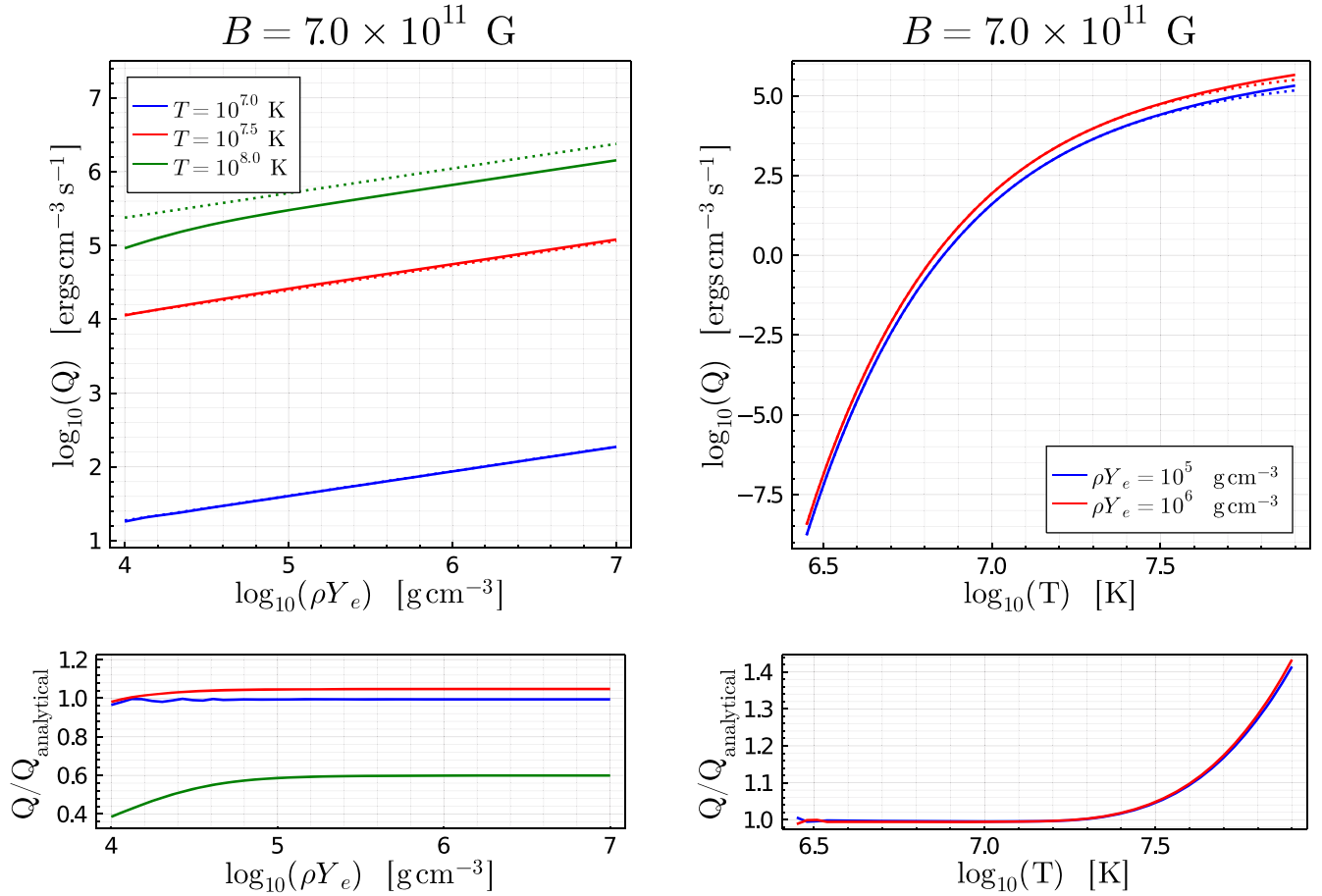

Figure 3. Synchrotron emission. Full numerical results (solid lines) from Equation (20) for the synchrotron emissivity as a function of density (left panel) and temperature (right panel). For comparison, we also display the analytic estimates (dotted lines) discussed in the text. In the left panel, we show the estimates for weak quantization from Equation (22b) (red and blue dotted), and non-quantization from Equation (22a) (green dotted). In the right panel, we show Equation (22b) and Equation (22a) at low and high temperatures, respectively.

Notice that all neutrino flavors are equally produced by the synchrotron process. It is useful to obtain two formulae that describe synchrotron emission in a regime relevant to WDs. We assume $T \ll m_e$, so that positrons can again be neglected ($f_+^\nu \ll f_-^\nu$). The degenerate limit $T \ll p_F^2/(2m_e) = E_F^{\rm NR}$ is valid, as $p_F \simeq (3\pi^2 n_e)^{1/3}$ for $\omega_B \ll E_F \simeq \mu$, and it is always large in WD cores (see Appendix A). The emissivity is

$$Q_{\rm syn}(\omega_B \ll T \ll E_F^{\rm NR}) = \left(\sum_{\nu_\alpha} C_A^2\right) \frac{G_F^2 \omega_B^6}{60\pi^3} \frac{3}{2} \frac{T}{E_F^{\rm NR}} n_e, \quad (22a)$$

$$Q_{\rm syn}(T \ll \omega_B \ll E_F^{\rm NR}) = \left(\sum_{\nu_\alpha} C_A^2\right) \frac{G_F^2 \omega_B^6}{60\pi^3} \frac{3}{2} \frac{\omega_B}{E_F^{\rm NR}} e^{-\omega_B/T} n_e. \quad (22b)$$

These limits are referred to as *non-quantized degenerate* and *weakly quantized degenerate*, respectively. In Figures 3 and 4, we display the full numerical results of Equation (20) together with the analytic estimates in Equations (22a) and (22b). The analytical approximation is precise up to large temperatures, where the energy loss should be interpolated between Equations (22a) and (22b). Given the strong dependence on the magnetic field, the analytical approximation of Equation (22b) is good enough to describe the region of transition from non-quantized to quantized,

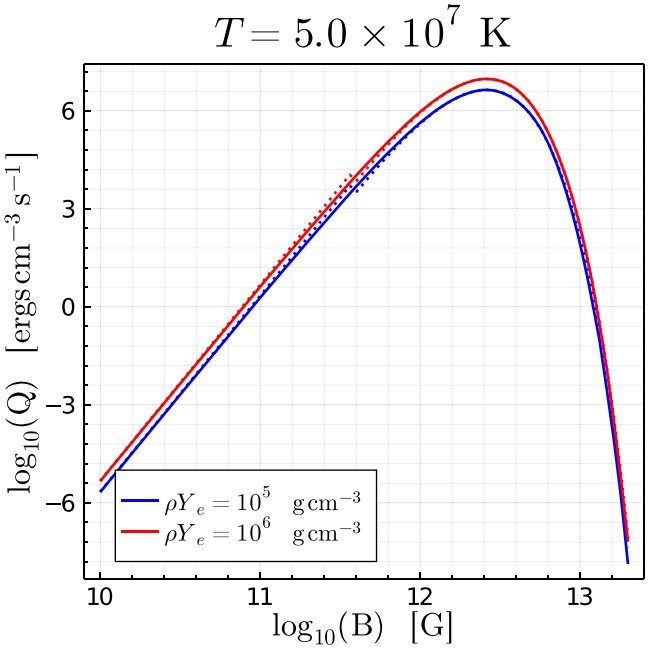

Figure 4. Magnetic dependence of synchrotron emission. Full numerical results from Equation (20) for synchrotron emission as a function of B for various densities. As before we show the analytic limits from Equations (22b) and (22a).

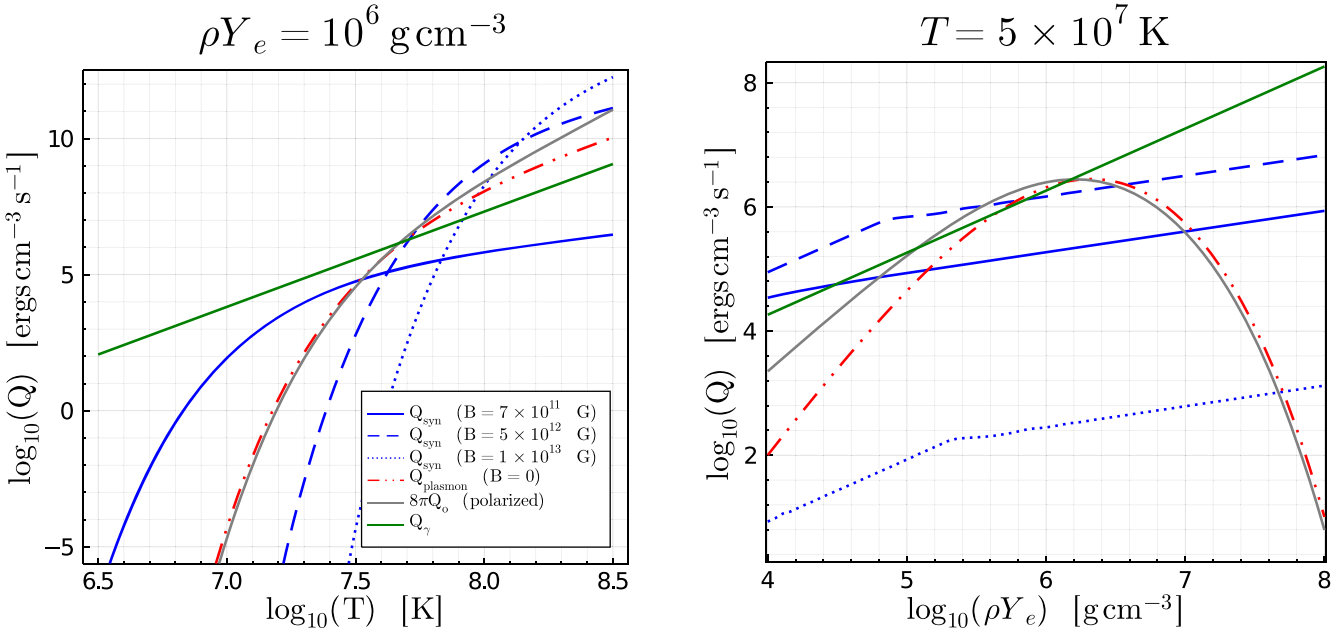

Figure 5. Magnetic fields and WD cooling. Magnetic field-induced cooling processes, including the emissivities due to synchrotron emission and plasmon decay in a polarized medium. For comparison, we also show the plasmon decay emissivity in the unmagnetized plasma, and the photon surface emissivity. Note that photon emission actually depends on the global properties of the star so Q_γ here is a volume average. We show the behavior as a function of temperature (left panel) and density (right panel).

considering our accuracy goals. Synchrotron emission is compared with all other processes in Figure 5, from which it can be seen that synchrotron emission can enhance the energy loss from WDs.

3.4. Heating from Magnetic Field Decay

Magnetic fields as large as those discussed in the previous sections can have additional effects on the evolution of a WD. One of them is the heating of the star due to ohmic decay of the magnetic field (Cumming 2002; Ferrario et al. 2015). The resulting conversion of the magnetic field energy[11] $U_{\rm em} = B^2/2$ into thermal energy is the dominant process in the evolution of a field smaller than 10^{12} G (Heyl & Kulkarni 1998). We do not attempt to quantify the potential effect of ohmic heating on the surface temperature at later stages (Valyavin et al. 2014), but instead only estimate it at the level of energy gain and loss per unit volume in the core in order to compare it to other processes discussed in this work. As an example, we consider a hypothetical magnetic field in the well-known WD G117-B15A, for which we take the parameters (Kepler et al. 2000; Bischoff-Kim et al. 2008)

$$Y_e\rho \simeq 10^6\ \mathrm{g\ cm^{-}3},\ R = 9.6\times10^8\ \mathrm{cm},\ T = 1.2\times10^7\ \mathrm{K}. \tag{24}$$

Assuming an exponential decay $B = B_0\exp(-t/t_{\rm ohm})$ with $t_{\rm ohm}\simeq 3\times10^{11}$ yr (Cumming 2002; Ferrario et al. 2015) and an age much smaller than $t_{\rm ohm}$, the energy density deposited by an initial magnetic field $B_0\simeq 3\times10^{11}$ G per unit of time is $-Q_{\rm ohm} = dU_{\rm em}/dt \simeq B_0^2/t_{\rm ohm} \simeq 750$ erg cm$^{-}3$ s^{-1}. Integrated over the volume, this corresponds to $\simeq 7\times10^{-4}L_\odot$. Comparing this to the energy loss due to neutrino cooling obtained from Equation (22b) with Equation (24), one finds $|Q_{\rm ohm}/Q_{\rm syn}|\simeq 7.6$, and hence, the additional heating by ohmic decay of the B would clearly dominate over the enhancement of the cooling rate caused by the B field. Moreover, the temperature would be larger due to the heating produced in previous times as well.

4. Applications and Discussion

In Figure 5, we show all the cooling processes discussed in this paper. Notice that at low temperatures neutrino bremsstrahlung is the dominant processes in neutrino production (Winget et al. 2004). However, this is a moot point, since at these temperatures, photon surface emission (which we display) becomes the dominant cooling process. We also notice in passing that the axial-vector contribution to plasmon decay in the presence of a magnetic field $B\simeq 5\times10^{12}$ G is subdominant compared to neutrino pair synchrotron radiation.

As a first application, we can notice that $n_e = Y_e\rho/m_u$, where m_u is the atomic mass unit. Therefore, the energy-loss rate due to synchrotron emission per mass unit reads, using the weakly quantized limit,

$$\epsilon_{\rm syn}^{\rm WD} \simeq \left(\sum_{\nu_\alpha} C_A^2\right)\frac{G_F^2\omega_B^6 Y_e}{60\pi^3 m_u}\frac{3}{2}\frac{\omega_B}{E_F^{\rm NR}}\exp[-\omega_B/T]. \tag{25}$$

Assuming $Y_e = 0.5$, $\rho = 2\times10^5\,\mathrm{g\,cm^{-3}}$, and $T\simeq 10^8\,\mathrm{K}\simeq 8.6\,\mathrm{keV}$, typical parameters for an RG core, we need the energy-loss rate per mass unit to be smaller than 10 erg g^{-1} s^{-1}, to prevent the cooling from delaying the onset of helium

[11] Note that we define the electromagnetic field energy density $U_{\rm em}$ using the particle physics-friendly rationalized units rather than the Gaussian *unrationalized* units of Chandrasekhar & Fermi (1953), i.e.,

$$U_{\rm em} = \frac{B^2}{2}, \tag{23}$$

rather than $U_{\rm em} = \frac{B^2}{8\pi}$ for the energy density of the B field. One can thus compute everything using natural units, and eventually substitute $1.95\times10^{-2}\,\mathrm{eV}^2 \to 1$ G, see also Appendix A of Raffelt (1996).

burning in the core (see Chapter 2 of Raffelt 1996). Intriguingly, recent works have advanced the hypothesis of a ubiquitous magnetic field in RG cores (Cantiello et al. 2016). We find that neutrino cooling constrains such a ubiquitous field to be smaller than the (arguably gargantuan) value $B_{\max} \lesssim 10^{12}$ G, where the approximation of negligible effect on the global structure might be already broken.

As a second application, let us consider the secular variation of their period of pulsation of stars like G117-B15A, which have been suggested to show an excessive cooling, prompting an axion production interpretation (Isern et al. 1992; Giannotti et al. 2016).[12] Using the parameters of Equation (24), we find that a field $B_{\max} \simeq 3 \times 10^{11}$ G produces a cooling of about $10^{-4} L_{\odot}$, which roughly matches the excessive cooling observed (Giannotti et al. 2016). We stress that this interpretation of the hint of cooling is far from conclusive, as the magnetic field should be totally confined in the core, something difficult to achieve (Peterson et al. 2021). A more careful analysis is demanded, but it could be important to further investigate an SM solution to the cooling hints, particularly in light of recent works, based on X-ray signals from axions reconverting in the magnetosphere of MWDs, challenging the axion hypothesis for this hint of cooling (Dessert et al. 2022).

As a third application, we investigate the potential to use the impact of B fields on neutrino emission to impose an upper bound $B_{\max}$ on the internal magnetic field in the WD population. Let us assume that all WDs have a magnetic field buried underneath their surface. For simplicity, we describe all the WDs as spheres with a fixed density and electron-to-baryon ratio of $\rho = 2 \times 10^6\,\mathrm{g\,cm^{-3}}$ and $Y_e = 0.5$. Moreover, we assume the magnetic field to have the same magnitude over the entire stellar core, with a sharp drop near the surface. If $B_{\max} \simeq 1.2 \times 10^{12}$ G, the neutrino energy loss, obtained from Equation (22b), is larger than that of the surface emission, given by Equation (7), for temperatures larger than 3.3×10^7 K. A value of $B_{\max} \simeq 6 \times 10^{11}$ G in WDs implies an energy loss of 10% of the surface emission at a core temperature of 2×10^7 K. This corresponds very roughly to a 10% effect on the WDLF. The argument above can be made slightly more precise by integrating the emissivities over a WD model, rather than assuming a constant value for the density profile (see Appendix C).

The effect of synchrotron radiation on stellar evolution could be analyzed more precisely through a code such as MESA (Paxton et al. 2011), together with experimentally determined WDLF. This would give more realistic constraints, properly including the density profile evolution of the WDs, as well as their mass distribution. The numerical implementation is possible thanks to Equations (22a) and (22b), which can be directly fed into a stellar evolution code, as the error due to the use of analytical approximations is never larger than a factor of $\mathcal{O}(1)$ at intermediate temperatures. Therefore, the analytical approximations are precise enough, since synchrotron radiation depends on a large (sixth) power of B. We leave this analysis for a future study.

Finally, as a very simple estimate, we compare the ohmic heating Q_{ohm} studied in Section 3.4 to Q_γ in Equation (7) and demand that the heating due to ohmic decay is less than 10% of the energy loss due to surface cooling (a number that would be of comparable magnitude to the cooling anomaly quoted in Giannotti et al. 2016, but of opposite sign). This translates into a bound of $B < 2.73 \times 10^{11}\mathrm{G}/\sqrt{Y_e}$ for the parameters in Equation (24). Notice however that heating depends on the ohmic decay time, and the bound on B roughly scales as $\propto \sqrt{t_{\mathrm{ohm}}}$. Therefore, if the lifetime of the magnetic field is larger than expected, the neutrino cooling bound applies, while if $t_{\mathrm{ohm}} \simeq 3 \times 10^{11}$ yr is a good estimate, the magnetic field is primarily constrained by the anomalous heating it would produce in this case. Unless a finely tuned cancellation happens between the heating due to the magnetic field decay and the cooling due to neutrino synchrotron radiation, these two constraints are complementary.

5. Conclusions

Besides affecting the global quantities of degenerate stars, strong magnetic fields could modify their cooling. A large magnetic field can catalyze the cooling by modifying the ordinary processes of a nonmagnetized core (Canuto et al. 1970a, 1970b; Galtsov & Nikitina 1972; DeRaad et al. 1976; Skobelev 1976; Kennett & Melrose 1998), and by introducing additional processes as the neutrino pair synchrotron radiation (Landstreet 1967; Iakovlev & Tschaepe 1981; Kaminker et al. 1992). We studied the impact of magnetic fields in the interior of RGs and WDs on neutrino cooling rates, which are constrained both at the population level via the WDLF and in individual stars for some WDs by pulsation measurements, and derived a new limit on the magnitude of the interior B fields. This independent limit complements several recent observations. Astrometric measurements suggest that most RGs could host very large magnetic fields (Fuller et al. 2015; Cantiello et al. 2016; Stello et al. 2016). Similarly, WDs could also hide large magnetic fields beneath their surfaces (Cantiello et al. 2016).

The problem of quantifying the impact that magnetic fields in stellar cores have on observable quantities factorizes into two parts: first identifying the relevant *microphysical* processes and computing their contributions to the emissivity, and second investigating the consequences that this has on the *macroscopic* structure of the WD and its evolution. In the present work, we focused on the first aspect. We found that the strongest effect on the cooling is due to synchrotron radiation, rather than to the modification of plasmon decay. Even without a detailed analysis of the stellar evolution, this leads to a stronger constraint on the B field than the well-known stability requirement. While this improvement only amounts to a factor of order one, the two constraints are complementary, as they depend on different observables, showing once more how particle production in stars can be a diagnostic tool for astrophysics.

More specifically, we found that if a ubiquitous magnetic field is present in RGs, it cannot be larger than 10^{12} G. From a comparison to the WDLF in the simple form of the Mestel cooling law, we have shown that a ubiquitous field hiding beneath WD surfaces needs to be smaller than 10^{12} G and could be potentially limited down to 6×10^{11} G, slightly improving the bounds coming from a stability requirement. Moreover, we found that variable stars like G117-B15A, which show excessive cooling, could be potentially affected by neutrino pair synchrotron radiation. However, we stress that the interpretation of the hints of cooling in terms of an internal magnetic field can be challenged, as such large magnetic fields should potentially show up in asteroseismological surveys.

[12] It has been argued that these hints point to an axion solution also because they are produced with a certain temperature dependence (Giannotti et al. 2016).

In addition to the impact that B fields can have on WD cooling, their ohmic decay can also heat the star's core. The energy gain due to this process can potentially exceed the loss from cooling by synchrotron radiation. Hence, the non-observation of excess heating can also impose an upper bound on B, which we estimate to be a factor of 2–3 stronger than the bound from the non-observation of excessive cooling due to synchrotron emission (assuming no cancellation between the two effects, which in reality would of course always coexist). A quantitative study, however, crucially relies on the details of B dissipation due to ohmic damping, which is beyond the scope of this work. The different parametric dependencies of the energy gain and loss caused by large B fields make these bounds complementary.

Our work could be expanded in several directions. One could study numerically the effect of synchrotron radiation on stellar evolution (through some code such as MESA; Paxton et al. 2011) with an experimentally determined WDLF to obtain a more precise bound on the internal magnetic field. Constraining the population of highly magnetized WDs would not only help better understand stellar evolution, but, e.g., also help estimate the gravitational wave background expected from very massive WDs (Kalita & Mukhopadhyay 2019). Finally, the production of some new elementary particles can be enhanced in the presence of large magnetic fields, thus providing an additional signature (Caputo et al. 2020; O'Hare et al. 2020; Caputo et al. 2021). For example, axion-like particles with an electron coupling can be produced via synchrotron radiation (Kachelriess et al. 1997). Such particles, if discovered, would open a new window into the internal magnetic fields of WDs.

E.V. thanks Georg Raffelt, Javier Redondo, Aldo Serenelli, and Irene Tamborra for discussions about related topics, and Matteo Cantiello for an important discussion on magnetic fields in stellar cores. We thank Matteo Cantiello, Georg Raffelt, and Irene Tamborra for their comments on the first version of the paper. Finally, we thank the anonymous referee for bringing the ohmic heating to our attention. J.I.M. is supported by the F. R.S.-FNRS under the Excellence of Science (EOS) project No. 30820817(be.h). The work of E.V. was supported in part by the U.S. Department of Energy (DOE) grant No. DE-SC0009937.

Appendix A
Plasmon Decay

We recollect here the main results of Braaten & Segel (1993), who found expressions for plasmon decay in isotropic and homogeneous plasmas for any condition.

A.1. Full Relativistic Results

The electron and positron distributions are

$$f_-(E) = \frac{1}{e^{(E-\mu)/T}+1}, \quad f_+(E) = \frac{1}{e^{(E+\mu)/T}+1}, \tag{A1}$$

where $E = \sqrt{p^2 + m_e^2}$, so that the net charge density

$$n_c = \frac{1}{\pi^2}\int_0^\infty dp\, p^2 (f_-(E) - f_+(E)) \tag{A2}$$

depends only on the chemical potential μ and the temperature T, which are therefore the two parameters upon which the QED plasma depends on when ion features are negligible. The dispersion relations for plasmons depend on the typical electron velocity

$$v_* = \frac{\omega_1}{\omega_p}, \quad v = \frac{p}{E}, \tag{A3}$$

where the plasma frequency is given by

$$\omega_p^2 = \frac{4\alpha}{\pi}\int_0^\infty dp \frac{p^2}{E}\left(1 - \frac{1}{3}v^2\right)(f_-(E) + f_+(E)), \tag{A4}$$

and

$$\omega_1^2 = \frac{4\alpha}{\pi}\int_0^\infty dp \frac{p^2}{E}\left(\frac{5}{3}v^2 - v^4\right)(f_-(E) + f_+(E)). \tag{A5}$$

The dispersion relations for transverse and longitudinal plasmons with energy ω and momentum k are, respectively,

$$\omega_t^2 = k^2 + \omega_p^2 \frac{3\omega_t^2}{2v_*^2k^2}\left(1 - \frac{\omega_t^2 - v_*^2k^2}{\omega_t^2}\frac{\omega_t}{2v_*k}\log\frac{\omega_t + v_*k}{\omega_t - v_*k}\right), \quad 0 \leqslant k < \infty \tag{A6}$$

and

$$\omega_l^2 = \omega_p^2 \frac{3\omega_l^2}{v_*^2k^2}\left(\frac{\omega_l}{2v_*k}\log\frac{\omega_l + v_*k}{\omega_l - v_*k} - 1\right), \quad 0 \leqslant k < k_{\max}, \tag{A7}$$

where $k_{\max}$ is the momentum at which the longitudinal plasmon dispersion relation crosses the light cone,

$$k_{\max} = \left[\frac{3}{v_*^2}\left(\frac{1}{2v_*}\log\frac{1+v_*}{1-v_*} - 1\right)\right]^{1/2}\omega_p. \tag{A8}$$

The total energy loss due to plasmon decay is given by

$$Q_{\gamma\to\nu\bar{\nu}} = Q_T + Q_A + Q_L, \tag{A9}$$

where the contribution from transverse plasmons through vector and axial-vector couplings, and from longitudinal plasmons through vector coupling, are, respectively,

$$Q_T = 2\left(\sum_{\nu_\alpha} C_V^2\right)\frac{G_F^2}{96\pi^4\alpha}\int_0^{+\infty} \times dk\, k^2 Z_t(k)(\omega_t^2 - k^2)^3 f_B(\omega_t), \tag{A10a}$$

$$Q_A = 2\left(\sum_{\nu_\alpha} C_A^2\right)\frac{G_F^2}{96\pi^4\alpha}\int_0^{+\infty} \times dk\, k^2 Z_t(k)(\omega_t^2 - k^2)\Pi_A(\omega_t, k)^2 f_B(\omega_t), \tag{A10b}$$

$$Q_L = \left(\sum_{\nu_\alpha} C_V^2\right)\frac{G_F^2}{96\pi^4\alpha}\int_0^{k_{\max}} \times dk\, k^2 Z_l(k)\omega_l^2(\omega_l^2 - k^2)^2 f_B(\omega_l), \tag{A10c}$$

where the plasmon distribution is given by

$$f_B(\omega) = \frac{1}{e^{\omega/T} - 1}. \tag{A11}$$

To compute them, one needs the functions renormalizing the coupling (Braaten & Segel 1993; Raffelt 1996),

$$Z_t(k) = \frac{2\omega_t^2(\omega_t^2 - v_*^2 k^2)}{3\omega_p^2\omega_t^2 + (\omega_t^2 + k^2)(\omega_t^2 - v_*^2 k^2) - 2\omega_t^2(\omega_t^2 - k^2)} \tag{A12}$$

for the transverse plasmon, and

$$Z_l(k) = \frac{2(\omega_l^2 - v_*^2 k^2)}{3\omega_p^2 - (\omega_l^2 - v_*^2 k^2)} \tag{A13}$$

for the longitudinal one. The axial-vector polarization function reads as

$$\Pi_A = \frac{2\alpha}{\pi}\frac{\omega^2 - k^2}{k}\int_0^\infty dp\frac{p^2}{E^2}\left(\frac{\omega}{2vk}\log\frac{\omega + vk}{\omega - vk} - \frac{\omega^2 - k^2}{\omega^2 - v^2k^2}\right)(f_-(E) - f_+(E)), \tag{A14}$$

where

$$\omega_A = \frac{2\alpha}{\pi}\int_0^\infty dp\frac{p^2}{E^2}\left(1 - \frac{2}{3}v^2\right)(f_-(E) - f_+(E)). \tag{A15}$$

A.2. Nonrelativistic Limit of Plasmon Cooling

In the nonrelativistic limit, the dispersion relations for transverse and longitudinal plasmons are, respectively,[13]

$$\omega_t^2 = \omega_p^2 + \boldsymbol{k}^2 \quad \text{and} \quad \omega_l^2 = \omega_p^2\,. \tag{A16}$$

The plasma frequency in the limit $T \ll m_e$ is given in terms of the electron density n_e by

$$\omega_p^2 = \frac{4\pi\alpha\, n_e}{m_e}\left[1 + \frac{1}{m_e^2}(3\pi^2 n_e)^{2/3}\right]^{-1/2} \simeq (20\ \mathrm{keV}\rho_6^{1/2})^2, \tag{A17}$$

where $\rho_6 = \rho/10^6\ \mathrm{g\,cm^{-3}}$, and we assumed $Y_e = 0.5$. We shall also make use of the approximations (valid for $T \ll m_e$) $Z_t \simeq 1$, $\Pi_A \simeq \omega_p^2/2m_e k(\omega^2 - k^2)/\omega^2$.

With this in mind we obtain the following approximations:

$$\begin{aligned} Q_T^{\mathrm{NR}} &\simeq 2\left(\textstyle\sum_{\nu_\alpha} C_V^2\right)\frac{G_F^2\omega_p^6}{96\pi^4\alpha}\int_0^{+\infty} dk\ k^2 f_B(\omega_t) \\ &\simeq \left(\textstyle\sum_{\nu_\alpha} C_V^2\right)\frac{G_F^2\omega_p^6}{24\pi^4\alpha}\zeta(3)T^3, \end{aligned} \tag{A18}$$

where in the second steps we approximate $\omega_t \simeq k$, and

$$\begin{aligned} Q_L^{\mathrm{NR}} &\simeq \left(\textstyle\sum_{\nu_\alpha} C_V^2\right)\frac{G_F^2}{96\pi^4\alpha}\int_0^{\omega_p} dk k^2\omega_p^2(\omega_p^2 - k^2)^2 f_B(\omega_p) \\ &\simeq \left(\textstyle\sum_{\nu_\alpha} C_V^2\right)\frac{G_F^2}{96\pi^4\alpha}\,\frac{T}{\omega_p}\,\frac{8\omega_p^9}{105}, \end{aligned} \tag{A19}$$

where in the second step we assume $\omega_p \ll T$. Notice however that for our conditions $\omega_p \simeq T$, so one should use the first equality as a good approximation. The axial-vector contribution is

$$\begin{aligned} Q_A^{\mathrm{NR}} &= 2\left(\textstyle\sum_{\nu_\alpha} C_A^2\right)\frac{G_F^2\omega_p^2}{96\pi^4\alpha}\int_0^{+\infty} dk\ k^2\Pi_A(\omega_t, k)^2 f_B(\omega_t) \\ &= 2\left(\textstyle\sum_{\nu_\alpha} C_A^2\right)\frac{G_F^2\omega_p^6}{96\pi^4\alpha}\int_0^{+\infty} dk\ \frac{k^4}{\omega_t^4}\frac{\omega_p^4}{4m_e^2} f_B(\omega_t). \end{aligned} \tag{A20}$$

We show the approximations from Equations (A18)–(A20) in Figure 1 from which we conclude that relativistic effects can be reasonably neglected for the regimes relevant for WDs.

That the agreement with nonrelativistic results being good is unsurprising, as can be seen by making the following estimates. If the WD is to be nonrelativistic and degenerate then $p_F \simeq (3\pi^2 n_e)^{1/3}$, which gives

$$p_F \simeq 515\ \mathrm{keV}(Y_e\rho_6)^{1/3}, \tag{A21}$$

with ρ_6 expressed in units $10^6\ \mathrm{g\,cm^{-3}}$ and Y_e is the number of electrons per baryon. The latter are related by $n_e = Y_e n_c = Y_e\rho/m_u$, where ρ is the mass density and m_u is the atomic mass unit. This corresponds (taking $Y_e\rho = 10^6\ \mathrm{g\,cm^{-3}}$) to a nonrelativistic Fermi energy $E_F^{\mathrm{NR}} = p_F^2/(2m_e) \simeq 200\ \mathrm{keV}$ (and it is actually even smaller, as the average density of the profile is about 15% of the central density (Shapiro & Teukolsky 1983). The highest temperatures of relevance here are $T \simeq 10^8\ \mathrm{K} = 8.621\ \mathrm{keV}$. Hence, we have that $E_F^{\mathrm{NR}} \ll m_e$ and $T \ll m_e$.

These approximations also allow us to understand the relative subdominance of the axial contribution. If we neglect logarithmic corrections, we can see that $Q_T/Q_A = \mathcal{O}(m_e^2T^2/\omega_p^4)$, therefore, finding that in a nonrelativistic and nonmagnetized plasma the emission through the axial-vector coupling is highly suppressed. As discussed in Raffelt (1996; see also Vitagliano et al. 2017), one can heuristically think of the plasmon decay as dipole radiation from electrons coherently oscillating in space, thus contributing to vector emission, while the axial-vector emission corresponds to electron spin flips. As spins do not oscillate coherently in an unpolarized medium, the emission rate is suppressed. This also implies that in the nonmagnetized medium plasmon decay produces mostly $\nu_e\bar{\nu}_e$ pairs (Vitagliano et al. 2017).

Appendix B
Virial Theorem, Stability, and Magnetic Field Strength

The virial theorem provides a general recipe to relate the time-averaged (denoted $\langle\cdot\rangle$) total kinetic energy of a system of particles, held together by interactions, with that of the total potential energy of the system,

$$2\langle T_{\mathrm{tot}}\rangle = n\langle V_{\mathrm{tot}}\rangle, \tag{B1}$$

where T is the kinetic energy and $V \propto r^n$ is the interaction bounding the system. For gravity $V = \Omega \propto r^{-1}$, one obtains a well-known result in mechanics. The generalization to a stellar environment that includes a magnetic field is immediate. One finds (Chandrasekhar & Fermi 1953; Shapiro & Teukolsky 1983; Coelho et al. 2014)

$$2\langle T\rangle + 3(\gamma - 1)\langle U\rangle + \langle\mathcal{M}\rangle + \langle\Omega\rangle = 0. \tag{B2}$$

[13] Notice that transverse plasmons have (in this limit) a dispersion relation resembling those of a massive particle. On the other hand, the dispersion relation of the longitudinal plasmon is such that its energy is independent of its momentum. Therefore, even in the nonrelativistic limit the comparison of plasmons to massive particles should not be taken too literally (Vitagliano et al. 2017).

Here, we separated the macroscopic motion of the fluid, T, from the kinetic energy associated with the temperature, $3(\gamma-1)\langle U\rangle$, where γ is defined by the polytrope of the gas, $P=K\rho^{\gamma}$, and ρ is the density of the system. As can be seen, the generalization simply requires us to substitute Ω with $\Omega+\mathcal{M}$, where $\mathcal{M}$ is the magnetic field energy. If there is no macroscopic motion and $\langle T\rangle=0$, the virial theorem requires

$$3(\gamma-1)\langle U\rangle+\langle\mathcal{M}\rangle+\langle\Omega\rangle=0, \tag{B3}$$

which combined with the definition of total energy

$$\langle E\rangle=\langle U\rangle+\langle\mathcal{M}\rangle+\langle\Omega\rangle, \tag{B4}$$

gives the requirement for dynamical stability

$$(3\gamma-4)(|\langle\Omega\rangle|-\langle\mathcal{M}\rangle)>0. \tag{B5}$$

In the absence of a magnetic field, a configuration is stable as far as $\gamma>4/3$. The presence of the magnetic field spoils stability once the energy associated with the magnetic field is larger than the gravitational potential. Explicitly we have

$$\Omega=-\frac{3}{5-n}\frac{G_N M^2}{R},\quad \mathcal{M}=\frac{1}{2}\int d^3x\,\langle B^2(x,t)\rangle, \tag{B6}$$

where we defined $n=1/(\gamma-1)$. Let us now find the maximum magnetic field which can be supported within a subregion of the star while maintaining stability.

Typically, magnetic field strengths can vary significantly between the outer layers and core of a WD (see, e.g., Kalita & Mukhopadhyay 2019). As stated in the main text, determining the precise magnetic field structure would entail modeling beyond the scope of this work. Nonetheless, the following toy setup is highly effective in illustrating how small magnetized core regions can affect cooling while remaining compatible with stability. Let us consider some prototype magnetic field profile

$$B=\begin{cases}B_{\rm core} & 0\leqslant r\leqslant R_{\rm core}\\ B_{\rm outer} & R_{\rm core}\leqslant r\leqslant R\end{cases} \tag{B7}$$

with $B_{\rm core}\gg B_{\rm outer}$. Then, an upper bound on the strength of the core magnetic field comes from the virial balance ($|\langle\Omega\rangle|=\langle\mathcal{M}\rangle$) and would give (in the nonrelativistic limit $\gamma=5/3$),

$$\begin{aligned}B_{\rm core}&\leqslant\frac{M}{R^2}\sqrt{\frac{18G_N}{4\pi(5-n)}}\left(\frac{R}{R_{\rm core}}\right)^{3/2}\\&=2.4\times10^8\frac{M}{M_\odot}\left(\frac{R_\odot}{R}\right)^2\left(\frac{R}{R_{\rm core}}\right)^{3/2}\,{\rm G},\end{aligned} \tag{B8}$$

where we assumed $M_\odot=1.99\times10^{33}\,{\rm g}$ and $R_\odot=6.96\times10^{10}\,{\rm cm}$. We assume $R_{\rm core}\simeq R$ in the following, with the magnetic field hidden just below the surface.

Let us now consider a canonical WD with a mass of around $0.6M_\odot$. From an observational point of view, this is well justified, as the WDs have a mass distribution peaked at a low mass (Weidemann & Koester 1984; Kepler et al. 2007) due to the combined effect of the progenitor initial mass function favoring small masses (Padmanabhan 2001), and to the nonlinear progenitor–WD mass relation, which also tends to favor WDs with small masses (Kalirai 2013). One also avoids the problems associated with the change in the structure of the large WD, due to the relativistic degenerate gas of electrons having $\gamma\simeq4/3$, which makes it very sensitive even to small magnetic fields (Shapiro & Teukolsky 1983).

For nonrelativistic electrons, the mass–radius relation is given by the simple result (see Equation (2.1) of Raffelt 1996, or Section 3.3 of Shapiro & Teukolsky 1983)

$$R=10,500\,{\rm km}\,(0.6M_\odot/M)^{1/3}(2Y_e)^{5/3}, \tag{B9}$$

and the central density is found to be

$$\rho_{\rm core}=1.46\times10^6\,{\rm g\,cm^{-3}}(M/0.6M_\odot)^2(2Y_e)^{-5}, \tag{B10}$$

where the mean molecular weight of the electrons is approximately $Y_e\simeq0.5$. Therefore, we find that the maximum B field allowed in WDs is

$$B_{\rm max}=8.8\times10^{11}(M/0.6M_\odot)^{1/3}\,{\rm G}. \tag{B11}$$

In principle, the magnetic field in the core could be larger than the one shown in Equation (B11). The density profile is a monotonically decreasing function of the radius, so a top-hat configuration could allow a larger magnetic field when applying the virial theorem to the core alone. Moreover, an analytical estimate is unavoidably rough, and does not account for several effects, which can potentially hinder the stability requirement bound. For example, Hamada & Salpeter (1961) showed as early as 1961 that Coulomb corrections and chemical composition can affect the mass–radius relations at the few tens of percent level. Most importantly, a more consistent treatment of the electron equation of state suggests that fields as large as $10^{13}\,{\rm G}$ for a $0.7M_\odot$ do not destabilize the star, and actually have a negligible effect on the mass–radius relation (Suh & Mathews 2000). Other authors have found smaller sustainable fields (Bera & Bhattacharya 2014; Franzon & Schramm 2015; Chatterjee et al. 2017). Therefore, we conclude that the bound on the internal magnetic field of WDs due to the stability requirement is somewhere between $B_{\rm max}\lesssim10^{12}\,{\rm G}$ and $B_{\rm max}\lesssim10^{13}\,{\rm G}$ with variability coming (among other things) from the spatial compactness of the higher fields within the star.

Appendix C
Integration Over the WD Profile

In this appendix, we show how the neutrino pair synchrotron emissivity can be integrated over a WD profile to refine the rough results shown in the main text. Given the precision we aim for, we can assume the WD to be isothermal, while the density profile can be found assuming hydrostatic equilibrium and the electron gas equation of state to be a polytrope in the low-density limit. This choice is consistent with the nonrelativistic approximations made throughout the paper, and the error introduced with respect to the exact equation of state (as well as relativistic and Coulomb corrections) is at most tens of percent for a $0.6\,M_\odot$ WD.

Since we have shown that for $\omega_B\gtrsim T$ the weakly quantized degenerate limit is a good approximation, we can easily integrate Equation (22b) over a density profile, assuming a constant magnetic field over the entire core with a sharp drop near the surface, and compare its temperature evolution to Equation (6),

$$L_\gamma=\vartheta L_\odot\frac{M}{M_\odot}T_7^{3.5}. \tag{C1}$$

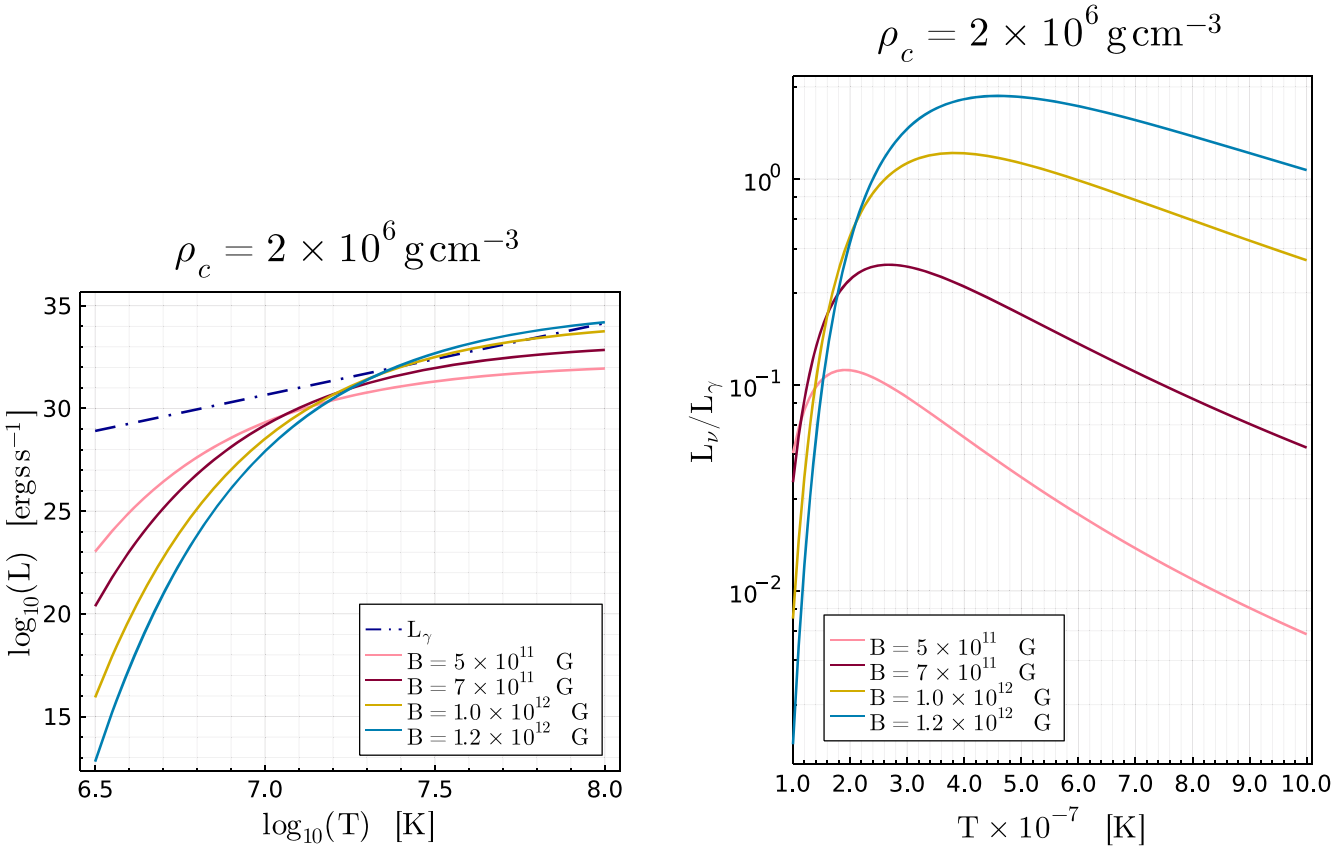

Figure 6. Comparison between surface luminosity and neutrino luminosity. Neutrino emissivities are integrated over a WD density profile with a central density $\rho_c = 2 \times 10^6$ g cm^{-3} for different values of the magnetic field. The ratio shown in the right panel peaks at larger temperatures as larger values of the magnetic field are assumed.

The results are shown in Figure 6. We see that compared to the constraint reported in the main text, we get slightly more stringent bounds on the internal magnetic fields when considering a $\mathcal{O}(1)$ effect on the cooling (1×10^{12} G, rather than 1.2×10^{12} G). With $B = 5 \times 10^{11}$ G we find a 10% effect. These results are easily explained by the dependence on the density of Equations (7) and (22b), since the first scales as ρ and the second as $\rho^{1/3}$. Therefore, the assumption of a constant density made in the main text is conservative. Notice however that the neutrino pair synchrotron emission is strongly dependent on the magnetic field, so the bounds eventually obtained assuming a fixed density over the WD and a more realistic profile will differ by tens of percent.

ORCID iDs

Marco Drewes https://orcid.org/0000-0003-0521-7586
Jamie McDonald https://orcid.org/0000-0002-9732-8330
Edoardo Vitagliano https://orcid.org/0000-0001-7847-1281

References

Abbott, L. F., & Sikivie, P. 1983, PhLB, 120, 133
Adams, J. B., Ruderman, M. A., & Woo, C. H. 1963, PhRv, 129, 1383
Agrawal, P., Bauer, M., Beacham, J., et al. 2021, EPJC, 81, 1015
Ai, W.-Y., Cruz, J. S., Garbrecht, B., & Tamarit, C. 2021, PhLB, 822, 136616
Angel, J. R. P. 1978, ARA&A, 16, 487
Angel, J. R. P., & Landstreet, J. D. 1970, ApJL, 160, L147
Angel, J. R. P., & Landstreet, J. D. 1971, ApJL, 164, L15
Antia, H. M., Chitre, S. M., & Thompson, M. J. 2000, A&A, 360, 335
Arias, P., Cadamuro, D., Goodsell, M., et al. 2012, JCAP, 06, 013
Baiko, D. A. 2009, PhRvE, 80, 046405
Baldner, C. S., Antia, H. M., Basu, S., & Larson, T. P. 2009, ApJ, 705, 1704
Barnabé, R., Strugarek, A., Charbonneau, P., Brun, A. S., & Zahn, J.-P. 2017, A&A, 601, A47
Bera, P., & Bhattacharya, D. 2014, MNRAS, 445, 3951
Bhattacharya, M., Mukhopadhyay, B., & Mukerjee, S. 2018, MNRAS, 477, 2705
Bischoff-Kim, A., Montgomery, M. H., & Winget, D. E. 2008, ApJ, 675, 1512
Braaten, E., & Segel, D. 1993, PhRvD, 48, 1478
Braithwaite, J., & Nordlund, Å. 2006, A&A, 450, 1077
Cantiello, M., Fuller, J., & Bildsten, L. 2016, ApJ, 824, 14
Canuto, V., Chiuderi, C., & Chou, C. K. 1970a, Ap&SS, 7, 407
Canuto, V., Chiuderi, C., & Chou, C. K. 1970b, Ap&SS, 9, 453
Caputo, A., Carenza, P., Lucente, G., et al. 2021, PhRvL, 127, 181102
Caputo, A., Millar, A. J., & Vitagliano, E. 2020, PhRvD, 101, 123004
Chandrasekhar, S. 1931, ApJ, 74, 81
Chandrasekhar, S., & Fermi, E. 1953, ApJ, 118, 116
Chanmugam, G., & Gabriel, M. 1972, A&A, 16, 149
Chatterjee, D., Fantina, A. F., Chamel, N., Novak, J., & Oertel, M. 2017, MNRAS, 469, 95
Coelho, J. G., Marinho, R. M., Malheiro, M., et al. 2014, ApJ, 794, 86
Córsico, A. H., Althaus, L. G., Miller Bertolami, M. M., Kepler, S. O., & García-Berro, E. 2014, JCAP, 08, 054
Couvidat, S., Turck-Chièze, S., & Kosovichev, A. G. 2003, ApJ, 599, 1434
Cox, J. P. 1980, Theory of Stellar Pulsation (PSA-2) (Princeton, NJ: Princeton Univ. Press)
Cumming, A. 2002, MNRAS, 333, 589
DeRaad, L. L., Jr, Milton, K. A., & Hari Dass, N. D. 1976, PhRvD, 14, 3326
Dessert, C., Long, A. J., & Safdi, B. R. 2022, PhRvL, 128, 071102
Di Luzio, L., Giannotti, M., Nardi, E., & Visinelli, L. 2020, PhR, 870, 1
Dine, M., & Fischler, W. 1983, PhLB, 120, 137
Dine, M., Fischler, W., & Srednicki, M. 1981, PhLB, 104, 199
Duez, V., Braithwaite, J., & Mathis, S. 2010, ApJL, 724, L34
Ferrario, L., de Martino, D., & Gänsicke, B. T. 2015, SSRv, 191, 111
Ferrario, L., Wickramasinghe, D., & Kawka, A. 2020, AdSpR, 66, 1025

Fowler, R. H. 1926, MNRAS, 87, 114
Franzon, B., & Schramm, S. 2015, PhRvD, 92, 083006
Friedland, A., & Gruzinov, A. 2004, ApJ, 601, 570
Fuller, J., Cantiello, M., Stello, D., Garcia, R. A., & Bildsten, L. 2015, Sci, 350, 423
Galtsov, D., & Nikitina, N. 1972, JETP, 35, 1047
Giannotti, M., Irastorza, I., Redondo, J., & Ringwald, A. 2016, JCAP, 05, 057
Giannotti, M., Irastorza, I. G., Redondo, J., Ringwald, A., & Saikawa, K. 2017, JCAP, 10, 010
Haft, M., Raffelt, G., & Weiss, A. 1994, ApJ, 425, 222
Hamada, T., & Salpeter, E. E. 1961, ApJ, 134, 683
Hansen, B. M. S., Richer, H., Kalirai, J., et al. 2015, ApJ, 809, 141
Harris, H. C., Munn, J. A., Kilic, M., et al. 2006, AJ, 131, 571
Heyl, J. S. 2000, MNRAS, 317, 310
Heyl, J. S., & Kulkarni, S. R. 1998, ApJL, 506, L61
Iakovlev, D. G., & Tschaepe, R. 1981, AN, 302, 167
Imoto, M., & Kanai, M. 1971, PASJ, 23, 363
Isern, J., Hernanz, M., & Garcia-Berro, E. 1992, ApJL, 392, L23
Jones, P. W., Pesnell, W. D., Hansen, C. J., & Kawaler, S. D. 1989, ApJ, 336, 403
Kachelriess, M., Wilke, C., & Wunner, G. 1997, PhRvD, 56, 1313
Kalirai, J. S. 2013, MemSAI, 84, 58
Kalita, S., & Mukhopadhyay, B. 2019, MNRAS, 490, 2692
Kaminker, A. D., Levenfish, K. P., Yakovlev, D. G., Amsterdamski, P., & Haensel, P. 1992, PhRvD, 46, 3256
Kantor, E. M., & Gusakov, M. E. 2007, MNRAS, 381, 1702
Kaplan, S. 1950, AJ, 27, 31
Kemp, J. C., Swedlund, J. B., Landstreet, J. D., & Angel, J. R. P. 1970, ApJL, 161, L77
Kennett, M. P., & Melrose, D. B. 1998, PhRvD, 58, 093011
Kepler, S. O., Kleinman, S. J., Nitta, A., et al. 2007, MNRAS, 375, 1315
Kepler, S. O., Mukadam, A., Winget, D. E., et al. 2000, ApJL, 534, L185
Kepler, S. O., Pelisoli, I., Jordan, S., et al. 2013, MNRAS, 429, 2934
Kohyama, Y., Itoh, N., Obama, A., & Hayashi, H. 1994, ApJ, 431, 761
Lai, D., & Shapiro, S. L. 1991, ApJ, 383, 745
Landstreet, J. D. 1967, PhRv, 153, 1372
Landstreet, J. D., & Bagnulo, S. 2019, A&A, 628, A1
Landstreet, J. D., Bagnulo, S., Valyavin, G. G., et al. 2015, A&A, 580, A120
Liebert, J., Bergeron, P., & Holberg, J. 2003, AJ, 125, 348
Liebert, J., Dahn, C. C., & Monet, D. G. 1988, ApJ, 332, 891
Loi, S. T., & Papaloizou, J. C. B. 2018, MNRAS, 477, 5338
Melrose, D. B. 1986, Instabilities in Space and Laboratory Plasmas (Cambridge: Cambridge Univ. Press)
Mestel, L. 1952, MNRAS, 112, 583
Meszaros, P., & Ventura, J. 1979, PhRvD, 19, 3565
Munn, J. A., Harris, H. C., von Hippel, T., et al. 2017, AJ, 153, 10
O'Hare, C. A. J., Caputo, A., Millar, A. J., & Vitagliano, E. 2020, PhRvD, 102, 043019
Padmanabhan, T. 2001, Theoretical Astrophysics, Vol. 2: Stars and Stellar Systems (Cambridge: Cambridge Univ. Press)
Pavlov, G. G., Shibanov, I. A., & Iakovlev, D. G. 1980, Ap&SS, 73, 33
Paxton, B., Bildsten, L., Dotter, A., et al. 2011, ApJS, 192, 3
Peccei, R. D., & Quinn, H. R. 1977, PhRvL, 38, 1440
Peterson, J., Dexheimer, V., Negreiros, R., & Castanheira, B. G. 2021, ApJ, 921, 1
Preskill, J., Wise, M. B., & Wilczek, F. 1983, PhLB, 120, 127
Prusti, T., de Bruijne, J. H. J., Brown, A. G. A., et al. 2016, A&A, 595, A1
Raffelt, G. G. 1986, PhLB, 166, 402
Raffelt, G. G. 1996, Stars as Laboratories for Fundamental Physics: The Astrophysics of Neutrinos, Axions, and Other Weakly Interacting Particles (Chicago, USA: Univ. Chicago Press)
Rowell, N., & Hambly, N. C. 2011, MNRAS, 417, 93
Shapiro, S. L., & Teukolsky, S. A. 1983, Black Holes, White Dwarfs, and Neutron Stars: The Physics of Compact Objects (New York: Wiley)
Sion, E. M., Holberg, J. B., Oswalt, T. D., et al. 2014, AJ, 147, 129
Skobelev, V. 1976, ZhETF, 71, 1263
Stello, D., Cantiello, M., Fuller, J., et al. 2016, Natur, 529, 364
Stix, T. H. 1962, The Theory of Plasma Waves (New York: McGraw-Hill)
Suh, I.-S., & Mathews, G. J. 2000, ApJ, 530, 949
Swanson, D. G. 2012, Plasma Waves (New York, NY: Elsevier)
Tremblay, P.-E., Fontaine, G., Fusillo, N. P. G., et al. 2019, Natur, 565, 202
Tsai, W.-y., & Erber, T. 1975, PhRvD, 12, 1132
Valyavin, G., Shulyak, D., Wade, G., et al. 2014, Natur, 515, 88
Vitagliano, E., Redondo, J., & Raffelt, G. 2017, JCAP, 12, 010
Weidemann, V., & Koester, D. 1984, A&A, 132, 195
Wickramasinghe, D. T., & Ferrario, L. 2000, PASP, 112, 873
Winget, D. E., Sullivan, D. J., Metcalfe, T. S., Kawaler, S. D., & Montgomery, M. H. 2004, ApJL, 602, L109
Yakovlev, D. G., Kaminker, A. D., Gnedin, O. Y., & Haensel, P. 2001, PhR, 354, 1
Zaidi, M. 1965, NCimA, 40, 502